THE UNIVERSITY OF MICHIGAN

College of Engineering

Department of Mechanical Engineering

Cavitation and Multiphase Flow Laboratory

Report No. UMICH 03371-4-T

A PHOTOGRAPHIC STUDY OF SPARK-INDUCED CAVITATION BUBBLE COLLAPSE

by

C. L. Kling *

F. G. Hammitt **

(Submitted for ASME presentation and publication)

Financial Support Provided by:

National Science Foundation

Grant No GK 13081

*Formerly, Doctoral Candidate, Nuclear Engineering Department, University of Michigan, Ann Arbor, Michigan. Present address: Combustion Engineering, Inc., Dept. 489, Windsor, Connecticut, 06095

*Professor-in-Charge, Cavitation and Multiphase Flow Laboratory, Mechanical Engineering Department, University of Michigan, Ann Arbor, Michigan, 48105.

July 1970

ABSTRACT

The collapse of spark-induced cavitation bubbles in a flowing system was studied by means of high speed photography. The migration of cavitation bubbles toward a nearby solid boundary during collapse and rebound was observed. Near its minimum volume the bubble typically formed a high speed microjet, which struck the nearby surface causing damage on selected target material.

ACKNOWLEDGEMENTS

Financial support for this work was provided under NSF Grants GK-730 and GK-13081 and ARO(D) Contract No. DAHOC4-67-0007.

LIST OF FIGURES

NOMENCLATURE

a	=	Time Scale Factor
b	=	Distance Between Bubble Centroid and Solid Boundary
$\dot{b}$	=	Bubble Centroid Velocity Toward Solid Boundary
$\ddot{b}$	=	Bubble Centroid Acceleration Toward Solid Boundary
E	=	Potential Enerby Available for Bubble Collapse
h	=	Initial Normalized Wall Distance; Initial Bubble Centroid-to-Wall Distance Divided by Maximum Bubble Radius
I	=	Electrical Current
ΔP	=	Difference Between Pressure at Infinity and the Bubble Total Internal Pressure at $R = R_{max}$
Q	=	Total Internal Pressure of Bubble at $R = R_{max}$
Q_g	=	Partial Pressure of Non-Condensable Gas in Bubble at $R = R_{max}$
R	=	Bubble Radius
R_o	=	Minimum Radius
R_{max}	=	Maximum Radius
$R_{1,2}$	=	Electrical Resistances
$\dot{R}$	=	Radial Velocity of Bubble Wall
$\ddot{R}$	=	Radial Acceleration of Bubble Wall
T_g	=	Absolute Temperature of Bubble Contents
V	=	Bubble Volume
$V_{1,2}$	=	Voltages
w	=	Exponential Decay Constant (time^{-1})

I. INTRODUCTION

Theoretical investigations of spherically symmetric cavitation bubble collapse starting with Rayleigh's classic ideal fluid analysis[1] indicate pressures in the liquid large enough to cause material damage; however, the precise method by which these pressures were applied against a solid surface remained vague. Recent investigations of spherically symmetric collapse which have included the effects of compressibility, internal gas,[2,3] viscosity and surface tension[3] have determined that with very low initial internal gas pressure potentially damaging pressures upon a nearby wall can be produced upon rebound. However, these pressures are only marginally damaging even at a distance from the collapse center less than or equal to the original bubble radius. The results of this experimental analysis show that for such wall proximity, spherical symmetry of collapse is not a valid assumption. Nevertheless, even if spherical symmetry were maintained, the bubble would need to be either initially attached to the wall or to migrate toward it during the collapse, and then rebound, in order to produce damage in the harder materials in which damage is actually observed. Fairly approximate theoretical investigations of the effect of a nearby solid boundary on bubble collapse[4,5] show that migration of the bubble centroid toward the wall does occur during collapse, but that the collapse rate becomes reduced when the initial bubble centroid is closer to the boundary. Obviously for such a collapse a strong asymmetry exists which will strongly affect bubble shape during collapse. Several theoretical analyses have been made, including two very recent comprehensive numerical treatments, to examine the effects of wall proximity[6,7,8], and in addition other asymmetrical conditions[7,8], upon bubble collapse profiles, velocities, and pressures. These analyses indicate the formation of a liquid jet during collapse which under certain conditions would be expected to impinge upon the wall with sufficient velocity to be an important damaging mechanism.

Photographic investigations of natural cavitation starting with the work of Sir Charles Parsons[9] have concluded that most observed damage at least includes a very strong mechanical component. Recent photographic studies[10, 11, 12, 13] indicate that only one bubble out of 10^4 to 10^{10}, appearing to collapse adjacent to a surface in a cavitation field, actually produces a damage pit. Therefore, the mechanism by which a bubble collapse produces damage must be highly selective. Several experimental studies[14, 15, 16, e.g.] have been conducted in recent years to determine the effect of a solid boundary on the collapse of attached or nearby bubbles in a static fluid. These studies show the formation of a liquid microjet produced by the deformation of the bubble wall due to the proximity of a solid surface. This microjet penetrates the bubble, striking the wall with sufficient velocity to be damaging in some cases.

The primary objective of the present study was to observe bubble collapse adjacent to a wall in a flowing system typical of actual engineering systems. In this way it might be possible to delineate those controlling parameters which separate the relatively very rare damaging bubble collapse from the relatively much larger number of non-damaging collapses, and perhaps begin to indicate methods of minimizing cavitation damage in flowing systems. Since the location of bubble collapse in such a system differs clearly from that of bubble growth, it is also possible to distinguish between pitting effects which may occur in either phase of bubble behavior. This distinction cannot easily be observed for the experiments in static systems. These objectives have been accomplished in a two dimensional cavitating venturi using bubbles generated by an electric spark upstream of, and at an adjustable distance from, a knife-edge wedge which bisects the venturi diffuser. A one-to-one correspondence between bubble collapses and craters on the wedge (for appropriate parameter settings) have been observed using a million frame per second camera.

II. EXPERIMENTAL EQUIPMENT

The experiments were conducted in a high-speed closed-loop water tunnel previously described.[17] Components particular to this investigation included a two-dimensional aluminum cavitating venturi inserted into the loop, a spark bubble-generator and a high-speed camera system. The reference pressure in the loop is maintained by regulating the cover air pressure in a surge tank, and flow rate is then controlled by pump speed adjustment. A by-pass loop containing a deionizer, filter, and cold-water vacuum deaerator was used for controlling impurity and air content. The latter was maintained at the minimum attainable of about 0.5 volume per cent at STP (about 0.3 of saturation at STP) so that the number of gaseous nuclei that could cause natural cavitation bubbles would be as small as possible. Pump speed and loop pressure were set so that natural cavitation was just suppressed in the aluminum test venturi. Flat glass (or plexiglas) windows could be installed in its sides. The constant dimension of the rectangular venturi cross section was parallel to the light beam used for photographing bubbles. Thus, the light beam was passed through a constant thickness of glass and water to reduce optical distortion.

A narrow stainless steel wedge was installed to bisect the angle of the diffuser, with its leading edge near the exit of the constant area throat section (Fig. 1). It could be moved axially as required. Flow equalization between the resulting two passages was attained by the use of downstream "spoilers" on either side of the wedge (Fig. 1.) The venturi had a throat cross-section 1.59 cm high x 1.27 wide x 5.08 cm long. The diffuser diverged at an initial included angle of 7^{o} for 5.0 cm downstream of the throat exit, and at an angle of 12^{o} thereafter. The initial angle of 7^{o} coincided with the included angle of the wedge thereby producing streamlines parallel to the wedge and diffuser wall. Axial wall

pressure profiles in the venturi were measured with removable side plates containing pressure taps. No pressure taps were used in the test section during the photographic runs.

The optical windows in the sides of the venturi were 17.2 cm long x 8.9 cm wide x 0.79 cm thick, and extended beyond either side of the throat. Attempts were made to use flat glass plates for optimum optical properties. However, the shock wave produced by the initial spark coupled with the clamping stresses in the glass plates caused severe breakage problems. Plexiglas plates of the same dimensions were then substituted to eliminate the breakage problems. These plates were drilled to accomodate the spark electrodes.
Their optical properties were adequate for the purpose. The spark electrodes consist of 0.075 cm hardened steel needles ground to a streamlined shape in the direction of flow.

Of the many possible methods to produce cavitation bubbles, the spark bubble generator was chosen because it is a simple devise which allows precise control of bubble size, bubble position, and time of initiation. The generator was made from a triggerable resistor-capacitor circuit with a time delay between the trigger pulse and the energy storage capacitor's discharge of about 5 μs and a pulse width of the discharge of about 1 μs. The bubble size was regulated by the magnitude of the energy storage capacitor, the charging voltage, and the magnitude of the damping resistor. Slight variations in these parameters from the generation of one bubble to the next produced about a 10% variation in bubble lifetime. An inductionless shunt resistor and voltage divider resistors were provided in the circuit for the measurement of electrical energy into the spark.

For several of the photographic studies, the stainless steel wedge was coated with a polished 50 μ thick aluminum foil (1100-0) with an adhesive

backing. This foil could be easily applied and removed. Because of its initial high polish, any deformation due even to a single impact could easily be detected. Photomicrographs were made of the damage pits produced by actual high-speed water jets, natural cavitation bubbles, and spark-induced shock waves and cavitation bubbles. A striking similarity in the craters thus produced was noted.

A Beckman and Whitley Model 330 camera with a framing rate adjustable between 10^4 and 2×10^6 frames/second was used for this investigation. The camera produces up to 80 frames/sequence and is capable of simultaneously producing a streak recording of the event. Because of the extremely short writing time (total number of frames/framing rate) at high speeds (40 μs at 2×10^6 frames/second), it was necessary to photograph the entire bubble lifetime ($\sim$1000 μs) at a low framing rate, and then use the higher framing rates to photograph a small portion of the bubble lifetime, usually near the final stages of collapse and initial stages of rebound. The camera utilizes a control system which provides the proper time delay between the event and the high intensity light source which illuminates the event. The camera control also regulates and records the camera framing rate.

III. EXPERIMENTAL RESULTS

A series of photographic-experimental runs were made to examine the effects of initial wall distance, bubble energy, and ambient pressure upon bubble collapse behavior and damaging potential. In all cases the liquid velocity at the location of the spark was about 25 m/sec and remained approximately constant along the bubble pathline because of the constant flow area provided by the geometry of the diffuser and wedge. Static pressure throughout this region was about 2 atm. (see Fig. 2 for typical wall pressure profiles with and without the wedge in place). A rather

comprehensive examination of the effects of the various pertinent parameters was made.[18] However, only a summary of typical results are included here.

From the photographic sequences, measurements were taken of the bubble size and position as it moved away from the electrodes and along the wedge. Since for similar parameter settings the bubble behavior was very repeatable (a 10% variation in bubble life-time, as previously mentioned was observed), the measurement of several sequences of similar bubbles was combined into a single data set.

Figs. 3 and 4 are selected frames from bubble collapse sequences of spark-induced bubbles with initial normalized wall distances, h of 1.62 and 1.14 respectively.

The general effect of a nearby solid boundary on the bubble collapse is shown in Table 1. As the initial normalized wall distance is decreased the proportionate decrease in wall distance increases and the relative minimum radius (ratio of final to initial radius) increases.

Finally an increasing fraction of the bubble collapse energy is transmitted to the high speed jet which is formed during collapse as normalized wall distance is decreased.

The high speed jet, generally directed toward the solid surface, is produced during collapse (and continues to exist during rebound) due to the asymmetric deformation of the bubble. Its velocity increases as the initial normalized wall distance is decreased so that the resultant "water hammer" pressure (Table 1) becomes adequate to explain the formation of single-impact craters in the soft aluminum coating of the steel wedge. A maximum "water hammer" pressure of 1745 atm. was calculated (Table 1).

Large high-contrast prints of the bubble collapse sequence shown in Fig. 4 were used to produce outlines of the bubble during collapse and rebound (Figs. 5-a and b, respectively). The outlines show that during the first phase of collapse, the restriction of fluid flow between the wedge and the bubble causes the bubble to elongate slightly along the axis perpendicular to the wedge. Later in the collapse, surface instabilities develop in the upper portion of the bubble. These instabilities result in a more rapid collapse of the upper portion of the bubble with the upper surface eventually moving through the bubble to form an irregular jet. In another case (Fig. 6) the surface instabilities become so large that the bubble actually divides in two before reaching minimum volume with each part then collapsing separately.

Since flow into the region between bubble and wall is restricted, the surface of the bubble closest to the wedge remains a nearly constant distance from the wedge during the collapse phase (Fig. 5). It does move toward the wedge after the bubble begins to rebound. Although this surface does not, the surface furthest from the wedge (and thus also the bubble centroid) does move toward the wedge during collapse. This movement of the centroid of the bubble produces a momentum directed toward the wall which must be conserved after minimum volume is reached. Therefore, the bubble and jet eventually may strike the surface of the wedge.

A direct comparison can be made between calculated bubble profiles for a bubble initially touching the wall[6] and our observed profile(for a bubble at a slightly greater distance from the wall, Fig. 5). The profiles are quite similar. The major difference appears to be that the computed profile becomes strongly oval about an axis normal to the wall, while only a slight distortion of this type appears in the actual

bubble. The observed profile flattens in a direction parallel to the wall at a relatively early phase of its collapse as compared to the computed profiles[6] either for a bubble initially attached to the wall or for one for which the collapse starts at a relatively substantial distance from the wall.

Fig. 7a shows the pit observed in the soft aluminum coating of the steel wedge under the point of collapse and rebound of the bubble in Fig. 4. This pit is very similar to a pit observed after the impingement of a high speed water jet (670 m/sec) on the same type of target material (Fig. 7b).[18] However, a very similar pit (Fig. 7c) was also observed under the position of the spark that initiated the bubble. This pit resulted from the impingement of the initial shock wave produced by the spark discharge, and is found under the electrodes rather than in the region of bubble collapse. The production of similar small pits under a planar shock wave was observed by Thomas[19] and attributed to local preferential "weak spots" in the material. Similar results were previously obtained by Thomas and Brunton.[20]

The damage produced by the collapsing bubbles on selected target materials appears very similar to the damage produced by both the impact of conventional high speed liquid jets and the impingement of a shock wave produced by initiation of the spark-induced bubbles. However, the damage patterns produced by the bubble collapse and conventional jet impingement were sometimes greatly asymmetric, depending presumably upon angle of impact, while in every case the damage pattern produced by the shock wave was very symmetric.

No pit was produced under the point of collapse and rebound for the bubble in Fig. 3, nor were pits observed for bubbles with an initial normalized wall distance < 1.0 (i.e., attached bubbles). Thus only a critical setting of the independent variables in this experiment will

produce damaging bubble collapses.

IV. ANALYSIS AND DISCUSSION

A. Motion of Bubble Centroid.

The motion of the bubble centroid during collapse can be approximated by the method of images[4] if the bubble is assumed to remain spherical. While this assumption is essentially indefensible for precise calculations, it can be used to obtain estimates of centroid motion which can then be compared with the photographs. More precise estimates of bubble motion require extremely complex analyses as those of Ref. 6, 7, and 8. In the present case the further assumption of an irrotational, incompressible, inviscid fluid was made. The radial collapse motion is then represented by a simple radial source, and the translational motion of the bubble centroid by a superimposed dipole source following the work of Cole.[21]

The resulting normalized equations for bubble motion are

$$\ddot{R} = \frac{1}{Rb\,(R+2b)} \left\{ \left[\frac{2Qa^2}{\Delta P} \left(\frac{1}{R} \right)^4 - 2a^2 - 3\dot{R}^2 + \frac{1}{2}\dot{b}^2 \right] b^2 - 2bR\dot{R}^2 + R^2 b\ddot{R} \right\} \qquad ---(9)$$

$$\ddot{b} = \frac{9}{16} \frac{R^3 \dot{b}^2}{b^4} - \frac{3\dot{R}\dot{b}}{R} - \frac{3}{2} \frac{R\dot{R}^2}{b^2} \qquad ---(10)$$

A special case of these equations for $b \to \infty$ results in a normalized differential equation:

$$\ddot{R} = \frac{\frac{Qa^2}{\Delta P} \left(\frac{1}{R} \right)^4 - a^2 - \frac{3}{2}\dot{R}^2}{R} \qquad ---(11)$$

which may be derived from the classical Rayleigh collapse equation with a provision for internal gas or vapor. These differential equations

were programmed on an analog computer. Figures 8a and b, and 9a and b are plots of the theoretical and experimental results for the bubbles shown in Figures 3 and 4 respectively. These curves show that the experimental and theoretical results agree very well in terms of the collapse rate and degree of migration toward the wall. Discrepancies during the growth of the bubble occur because of the effect of after-flow produced by the emission of a shock wave when the bubble was initiated. Also, because of the first order nature of the solution the theoretical bubble migration toward the solid boundary takes place over a shorter period than the experimental measurements.

B. Spark Bubble Characteristics.

Although spark-generated bubbles have been used by numerous investigators for the study of cavitation[14, 15, eg.], it is obvious that they differ in potentially important aspects from true cavitation bubbles. It is then desirable to examine the characteristics of the spark bubble more closely at this point.

The discharge of a short duration underwater spark results in a high pressure, high temperature plasma. Mechanical work, light radiation, thermal radiation, and thermal conduction dissipate energy from the plasma. The initial high pressure results in the radiation of a shock wave which has been estimated to contain 20% to 50% of the initial energy.[22] After emission of this shock wave, although the internal pressure is still well above the hydrostatic pressure, the bubble motion may be reasonably approximated by incompressible theory. As the bubble expands the internal pressure eventually drops below hydrostatic. However, due to inertia, outward motion will continue. Finally the pressure deficit between the hydrostatic liquid pressure and the internal gas and vapor pressures arrests the bubble wall motion and collapse begins. Velocities and pressures during the collapse and subsequent rebound may result in large enough secondary pressure pulses

or shock waves so that water compressibility must be considered.

Total energy dissipated in the spark, E_s, can be determined using the relation:

$$E_s = \int_o^\infty VI\, dt \qquad ---(12)$$

V and I were measured simultaneously in the present tests, using the voltage divider and shunt resistors of the spark generator circuit. Since the discharge circuit is a simple RC circuit, the displayed voltages across the resistors may be approximated by an exponential. Using a 100:1 voltage divider and integrating Eq. 1:

$$E_s = \frac{100\, V_{o2}\, V_{o4}}{2\omega R_2} \qquad ---(13)$$

where $I = \frac{V_2}{R_2} = \frac{V_{o2}}{R_2}\, e^{-\omega t}$

Results of the measurements taken show (Table 2) that depending upon the damping resistor and to a smaller degree on the relative sizes of the hold-off gap versus the water gap, only 0.5% to 10% of the total energy stored in the capacitor is actually dissipated in the water to produce the spark bubble. For these measurements, which were correlated with the photographs of spark bubbles, the maximum potential energy of the bubble is given by:

$$E_p = \frac{4}{3}\, \pi\, R_{max}^3\, \Delta P \qquad ---(14)$$

E_p varies between 0.50 and 0.30 of the energy dissipated in the water (Table 2). Therefore 0.50 to 0.70 of this energy is dissipated by thermal radiation and conduction, by the production of a pressure or shock wave, and by the formation of permanent gas.

The hydrostatic pressure differential, ΔP, the maximum radius, R_{max}, and the minimum radius, R_o may be measured for typical cases. Thus estimates of the total internal pressure, Q, at $R = R_{max}$ can be made. Equating the maximum potential energy of the bubble (Eq. 14) to the energy of expanding the bubble from its minimum to its maximum volume

$$E = \frac{4}{3} \pi \Delta P R_{max}^3 = \int_{R_o}^{R_{max}} P dV = 4\pi \int_{R_o}^{R_{max}} P R^2 \, dR \qquad ---(15)$$

and assuming adiabatic expansion

$$P = Q \left(\frac{R_{max}}{R} \right)^4 \qquad ---(16)$$

results in

$$Q = \frac{\Delta P}{3 \left(\frac{R_{max}}{R_o} - 1 \right)} \qquad ---(17)$$

Using Eq. 16 again, the maximum pressure, P_o, in the bubble at minimum volume is:

$$P_o = \frac{\Delta P}{3} \quad \frac{(R_{max}/R_o)^4}{(R_{max}/R_o - 1} \qquad ---(18)$$

An estimate of the amount of gas formed during the spark discharge can be made by assuming:

1) Permanent gas is formed by the dissociation of water into hydrogen and oxygen gas with no recombination.
2) About 0.50 of the spark energy dissipated in the water goes into gas formation (assumed from measurements in Table 2).

3) The temperature of the gas at R_{max} is the ambient water temperature. With these assumptions the partial pressure of the permanent gas, Q_g (atm), is given by:

$$Q_g = 0.1025 \frac{E_{in} T_g}{R^3} \qquad \text{---(19)}$$

where E_{in} = energy dissipated in gas formation

For typical bubbles the partial pressure of the permanent gas is approximately half of the total internal pressure (Eq. 17) at maximum volume (Table 2). This partial pressure of permanent gas, which is the same order of magnitude as the water vapor pressure (0.025 atm), is thus much higher than the partial pressure expected from the naturally occurring gas nuclei present in the water tunnel facility.[23] This estimate of the permanent gas may be quite high due to the assumptions made. However, the possibility of a substantial amount of permanent gas formation in a spark bubble is shown, and a large amount of superheated water vapor may also be formed which conceivably may affect bubble collapse. If so, the damage potential of a spark generated bubble could be much less than that of a natural cavitation bubble which collapses in the same hydrostatic pressure and contains little or no permanent gas. A more recent study of this situation[24] appears to indicate that spark bubbles collapsing under the relatively high pressures here existing should behave essentially the same as natural cavitation bubbles under these conditions.

V. CONCLUSIONS

The theoretical and experimental evidence presented show the effects of a nearby solid boundary on the collapse of natural and spark-induced cavitation bubbles. The primary effect is the substantial movement of the centroid of the bubble toward this boundary. In many cases the distance between the inner bubble wall and the solid boundary remains approximately constant during collapse, but the outer bubble wall moves rapidly toward the solid boundary. For bubbles initially sufficiently close to this boundary, the bubble continues to move toward the wall during rebound and eventually strikes it.

Another effect of the solid boundary is to change drastically the collapse mode of the bubble. Although the bubble is nearly spherical at maximum volume, large asymmetries produced during collapse generally result in a high speed jet which pierces the bubble and in some cases strikes the nearby solid boundary with sufficient velocity to cause individual craters in soft aluminum.

The damage produced by the collapsing bubbles on selected target materials is very similar in appearance to the damage produced by both the impact of conventional high speed liquid jets and the impingement of a shock wave produced by initiation of the spark-induced bubbles. However, the damage patterns produced by the bubble collapse and conventional jet impingement were sometimes greatly asymmetric, depending presumably upon angle of impact, while in every case the damage pattern produced by the shock wave was very symmetrical.

The damage potential produced by the collapse of a cavitation bubble is very sensitive to the position of the bubble relative to the solid boundary, and to the volume ratio of collapse before asymmetries cause formation of the high speed jet. Maximum damage potential is achieved when the jet does not form until minimum volume is approximately attained, and when the bubble has migrated sufficiently so that the jet immediately strikes the boundary.

BIBLIOGRAPHY

1. Lord Rayleigh, "On the Pressure Developed in a Liquid During Collapse of a Spherical Cavity", Phil. Mag., 34, (1917), pp. 94-98.

2. R. Hickling and M. S. Plesset, "Collapse of a Spherical Cavity in Water", Phys. of Fluids, 7, 1, (1964), pp. 7-14.

3. R. D. Ivany and F. G. Hammitt, "Cavitation Bubble Collapse in Viscous Compressible Liquid-Numerical Analysis", Trans. ASME, J. Basic Engr., D, 87, 4, (1965), pp. 977-985.

4. A. N. Korovkin, Y. L. Levkovskiy, "Investigation of the Collapse of a Cavitating Bubble Near a Solid Wall", Inzhenernofizicheskiy zhurnal, 12, 2, (1967), pp. 246-253.

5. A. Shima, "The Behavior of a Spherical Bubble in the Vicinity of a Solid Wall", Trans. ASME, J. of Basic Engr., 90, (1968), pp. 109-144.

6. R. B. Chapman, "Nonspherical Vapor Bubble Collapse", Ph. D. thesis, California Institute of Technology, 1970. See also M. S. Plesset and R. B. Chapman, "Collapse of an Initially Spherical Vapor Cavity in the Neighborhood of a Solid Boundary", California Inst. of Tech., Division of Engr. and Applied Science, Report No. 85-49, June 1970; see also CIT Rept. 85-81, R. B. Chapman, M. S. Plesset.

7. T. M. Mitchell, Ph. D. thesis, (in progress), Nuclear Engineering Department, The University of Michigan.

8. T. M. Mitchell and F. G. Hammitt, "Collapse of a Spherical Bubble in a Pressure Gradient", 1970 Cavitation Forum, May 24-27, 1970, Detroit, Michigan, pp. 44-46.

9. L. C. Burrill, "Sir Charles Parsons and Cavitation", Trans. Inst. Marine Engrs., 43, 8, (1951), pp. 149-167.

10. M. S. Plesset, "Shockwaves from Cavity Collapse", Phil. Trans., Roy. Soc., (London), A, 1110, 260, July 1966, pp. 241-244.

11. H. G. Olson, "High Speed Photographic Studies of Ultrasonically-Induced Cavitation and Detailed Examination of Damage to Selected Materials", Doctoral Dissertation, Dept. of Nuclear Engr., University of Michigan, August 1966. Also available as ORA Report 07738-2-T, University of Michigan, August 1966.

12. M. J. Robinson, "On the Detailed Flow Structure and the Corresponding Damage to Test Specimens in a Cavitating Venturi", Ph. D. thesis, Dept. of Nuclear Engineering, Laboratory of Fluid Flow and Heat Transport Phenomena, University of Michigan, 1965.

13. M. J. Robinson and F. G. Hammitt, "Detailed Damage Characteristics in a Cavitating Venturi", Trans. ASME, J. Basic Engr., D, 89, 1, (1967), pp. 161-173.

14. C. F. Naude and A. T. Ellis, "On the Mechanism of Cavitation Damage by Non-Hemispherical Cavities Collapsing in Contact with a Solid Boundary", Trans. ASME, J. Basic Engr., D, 83, 4, (1961), pp. 648-656.

15. N. D. Shutler, R. B. Mesler, "A Photographic Study of the Dynamics and Damage Capabilities of Bubbles Collapsing Near Solid Boundaries", Trans. ASME, J. Basic Engr., D, 87, 2, (1965), pp. 511-517.

16. T. B. Benjamin, "Cavitation in Liquids", Doctoral Dissertation, Cambridge University, 1954.

17. F. G. Hammitt, "Cavitation Damage and Performance Research Facilities", Symposium on Cavitation Research Facilities and Techniques, ASME, (1964), pp. 175-184.

18. C. L. Kling, "A High Speed Photographic Study of Cavitation Bubble Collapse", Doctoral Dissertation, Dept. of Nuclear Engineering, University of Michigan, 1970; also available as ORA Report 03371-2-T, University of Michigan, March, 1970.

19. G. P. Thomas and J. H. Brunton, "Drop Impingement Erosion of Metals", Proc. Roy. Soc. (London), A, 314, (1970), pp. 549-565.

20. G. P. Thomas, "The Initial Stages of Deformation in Metals Subjected to Repeated Liquid Impact", Phil. Trans. Roy. Soc., A, 1110, 260, (July 1966), pp. 140-143.

21. R. H. Cole, Underwater Explosions, Princeton University Press, 1948.

22. M. I. Vorotnikova, "Effect of the Heat-Emission Rate in an Underwater Electric Explosion on the Distribution of the Explosion Energy", Zhurnal prkladnoy mekhaniki i tekhnicheskoy fiziki, No. 2, (1962), pp. 110-112.

23. O. Ahmed, Ph. D. thesis, (in progress), Department of Nuclear Engineering, University of Michigan.

24. D. C. Gibson, "The Kinetic and Thermal Expansion of Vapour Bubbles", CSIRO, Division of Mechanical Engineering, Melbourne, Australia; 1970.

TABLE 1

Spark Generated Cavitation Bubble Parameters

Bubble Number	3	---	---	4
Maximum Radius, R_{max} (mm)	2.01	2.21	2.01	2.02
(normalized)	(1.0)	(1.0)	(1.0)	(1.0)
Initial Wall Distance, h (mm)	3.26	3.10	2.42	2.29
(normalized)	(1.62)	(1.40)	(1.21)	(1.14)
Partial Gas Pressure at $R = R_{max}$ (atm)	0.129	0.108	0.114	0.136
Minimum Radius, R_o (mm)	0.261	0.376	0.393	0.472
(normalized)	(0.129)	(0.171)	(0.195)	(0.233)
Wall Distance at $R = R_o$ (mm)	2.67	2.29	1.08	0.88
(normalized)	(1.33)	(1.03)	(0.54)	(0.44)
Pressure Inside Bubble (atm) at $R = R_o$	455.0	130.0	76.0	44.3
Jet Impingement Velocity (m/s)	none	35.4	73.2	120.0
Water Hammer Pressure (atm)	---	514.0	1063.0	1745.0

Bubble Number refers to corresponding figure number of this paper.

TABLE 2

Energy and Pressure Calculations for the Under-Water Spark Bubble Generator

Air Gap (mm)	3.0	3.0	3.0	3.0	3.0	2.8	2.8	2.8
Under Water Gap (mm)	1.0	1.0	0.5	0.5	0.5	1.3	1.0	0.7
Damping Resistor (ohms)	0	0	0	22	510	0	22	22
Capacitor Energy (jóules)	0.415	0.500	0.500	0.245	0.500	1.500	0.186	0.245
Energy Deposited in Water (jóules)	0.0327	0.0295	0.0210	0.0031	0.0031	0.1785	0.0125	0.0134
Percentage	7.87	5.90	4.28	3.32	0.611	11.9	6.73	5.47
Bubble Potential Energy (jóules)	0.0113	0.0136	0.0089	0.0034	0.0013	0.0899	0.0057	0.0058
Percentage	2.48	2.72	1.78	1.37	0.268	5.99	3.08	2.39
Ambient Pressure (atm)	3.27	1.18	1.18	1.08	1.16	0.303	0.815	1.67
Partial Pressure (atm) at $R = R_{max}$ (Eq. 19) due to permanent gas	0.0623	0.0222	0.0179	0.0169	0.0171	0.0086	0.0157	0.0228
Total Internal Gas Pressure at $R = R_{max}$ (atm) (Eq. 17)	0.124	0.0453	0.0486	0.0328	0.0218	0.0104	0.0325	0.0621

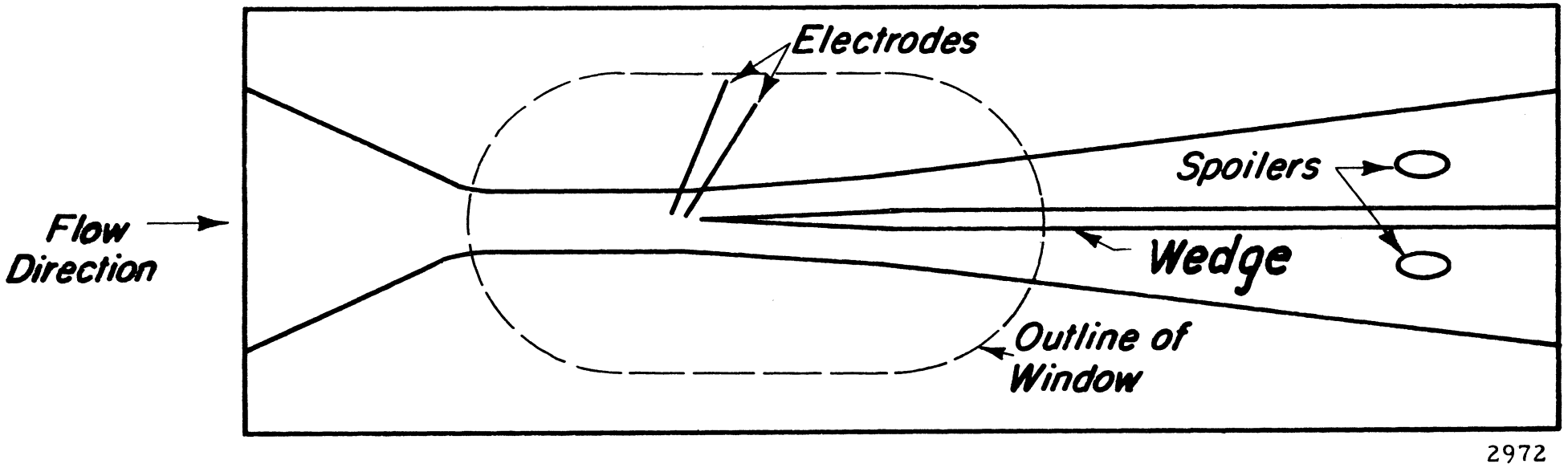

Figure 1. Schematic Diagram of Original and Modified Flow Path for the Aluminum Two-Dimensional Venturi Including Wedge and Spoilers

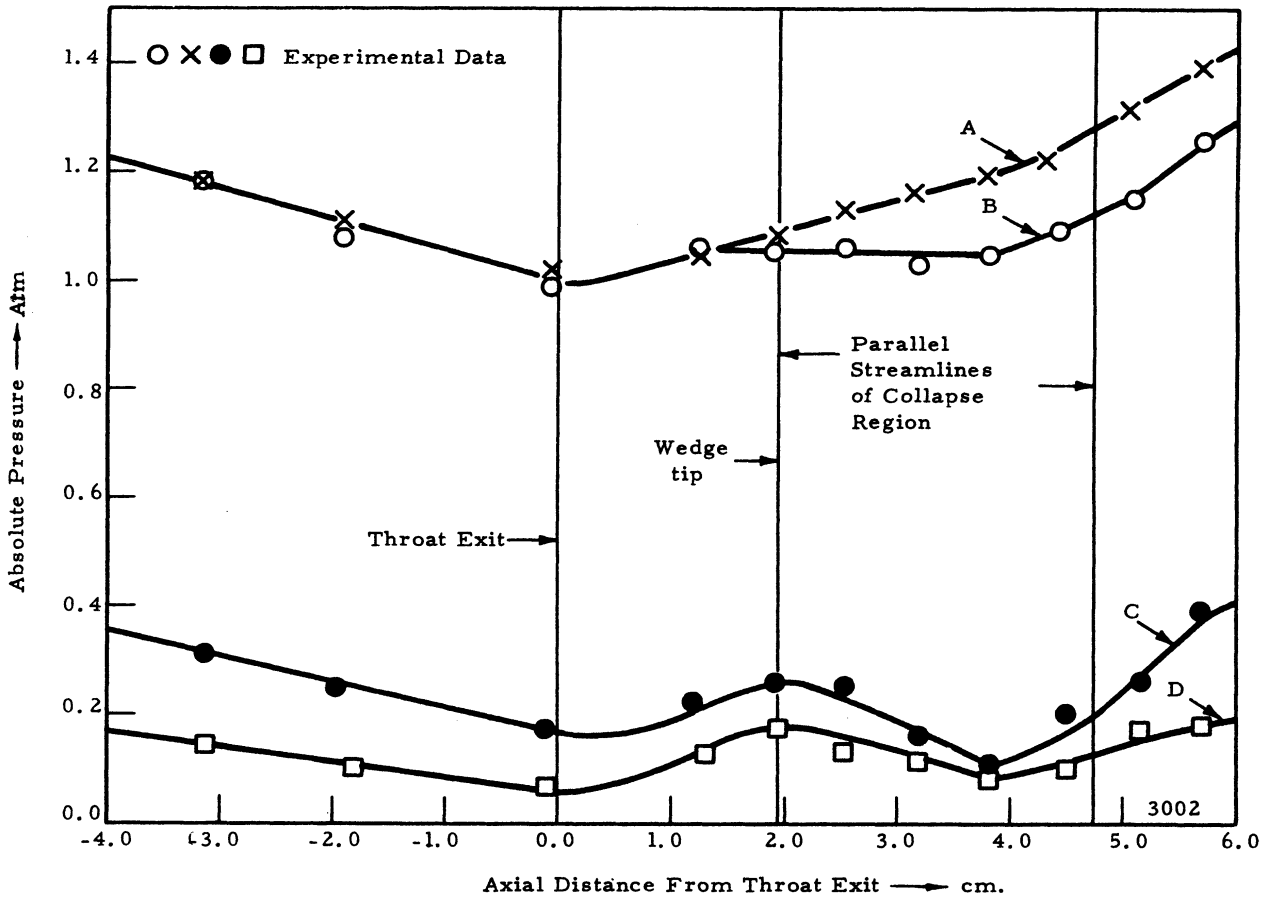

Figure 2. Typical Axial Pressure Profiles for the Modified Aluminum Two-Dimensional Venturi with and without the Wedge in Place; A and C: without wedge in place; B and D: with wedge in place.

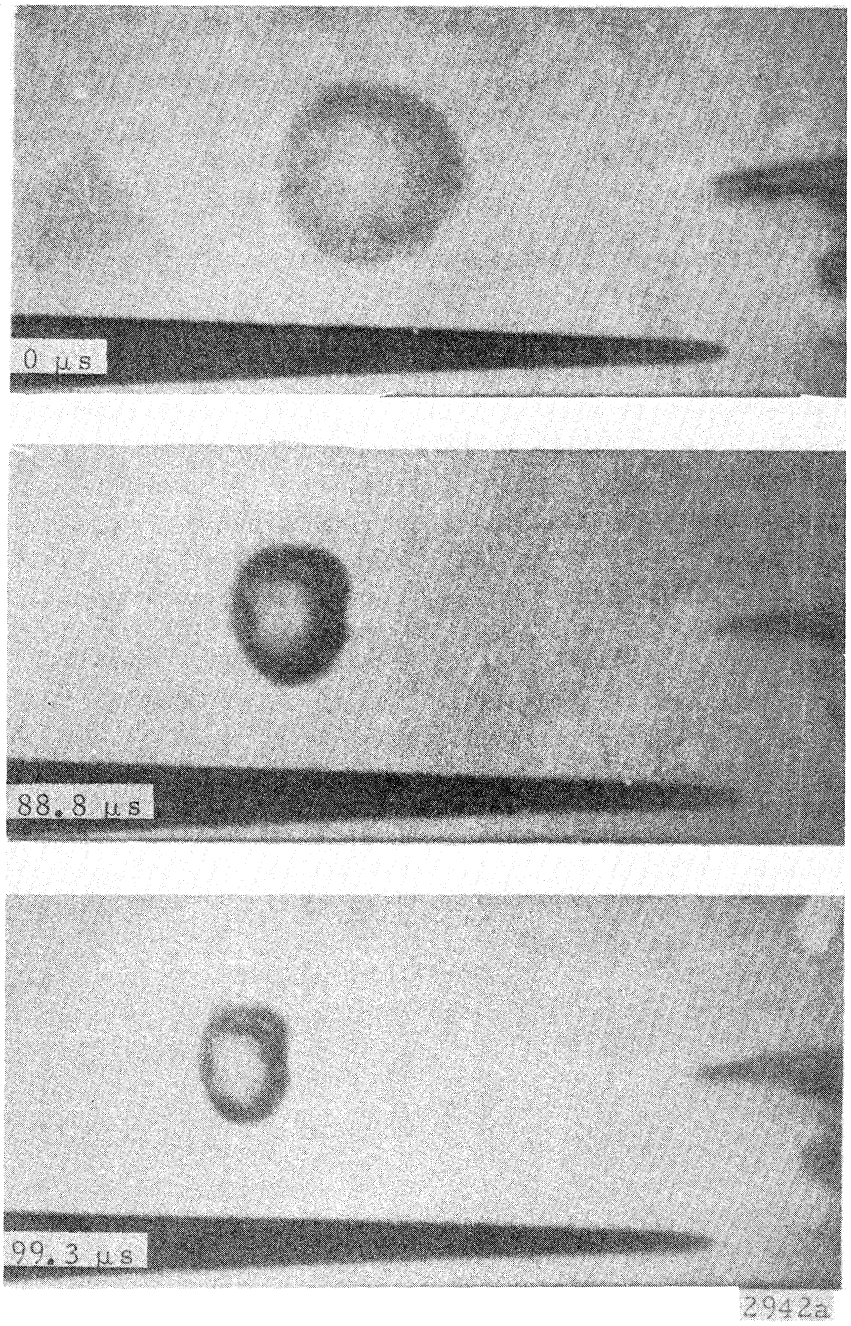

Figure 3a. Model 330 High Speed Photographs of a Spark Induced Cavitation Bubble Collapsing in the Modified Aluminum Two-Dimensional Venturi. Diffuse Back Lighting, Time Measured from First Frame, 0.8 μs Exposure/Frame Fluid Velocity 26.7 m/s, Right to Left, Initial Normalized Wall Distance, $h = 1.62$, Magnification 5.0, Air Content 0.8%.

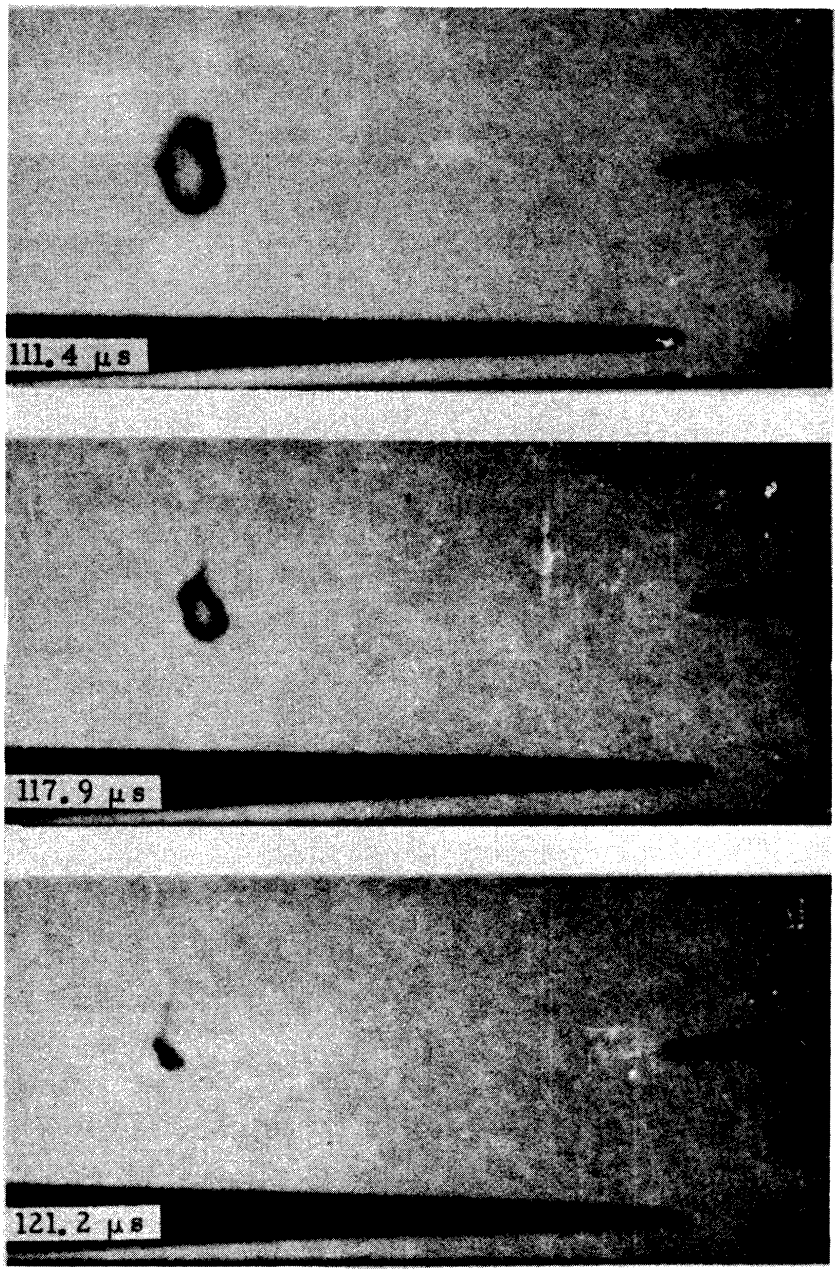

2942b

Figure 3b. Continued

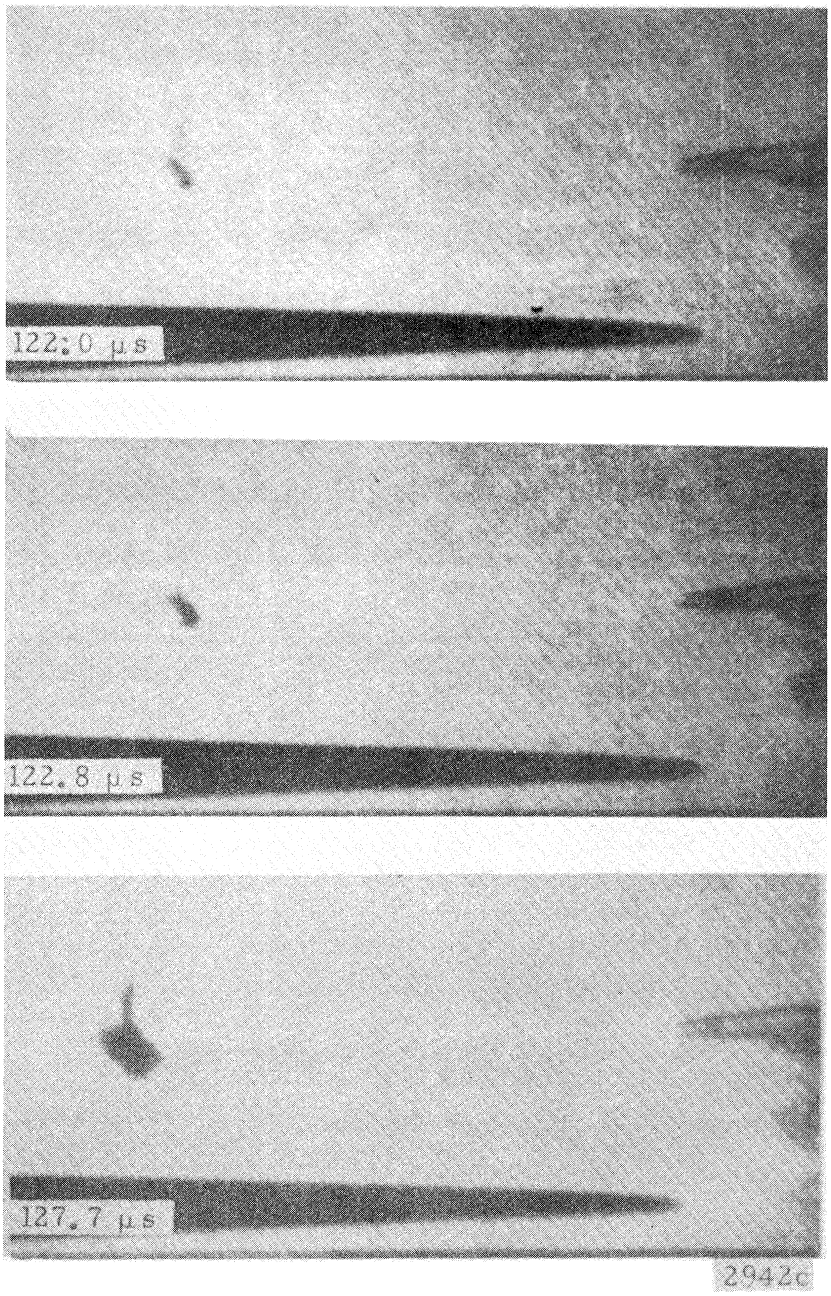

Figure 3c. Continued.

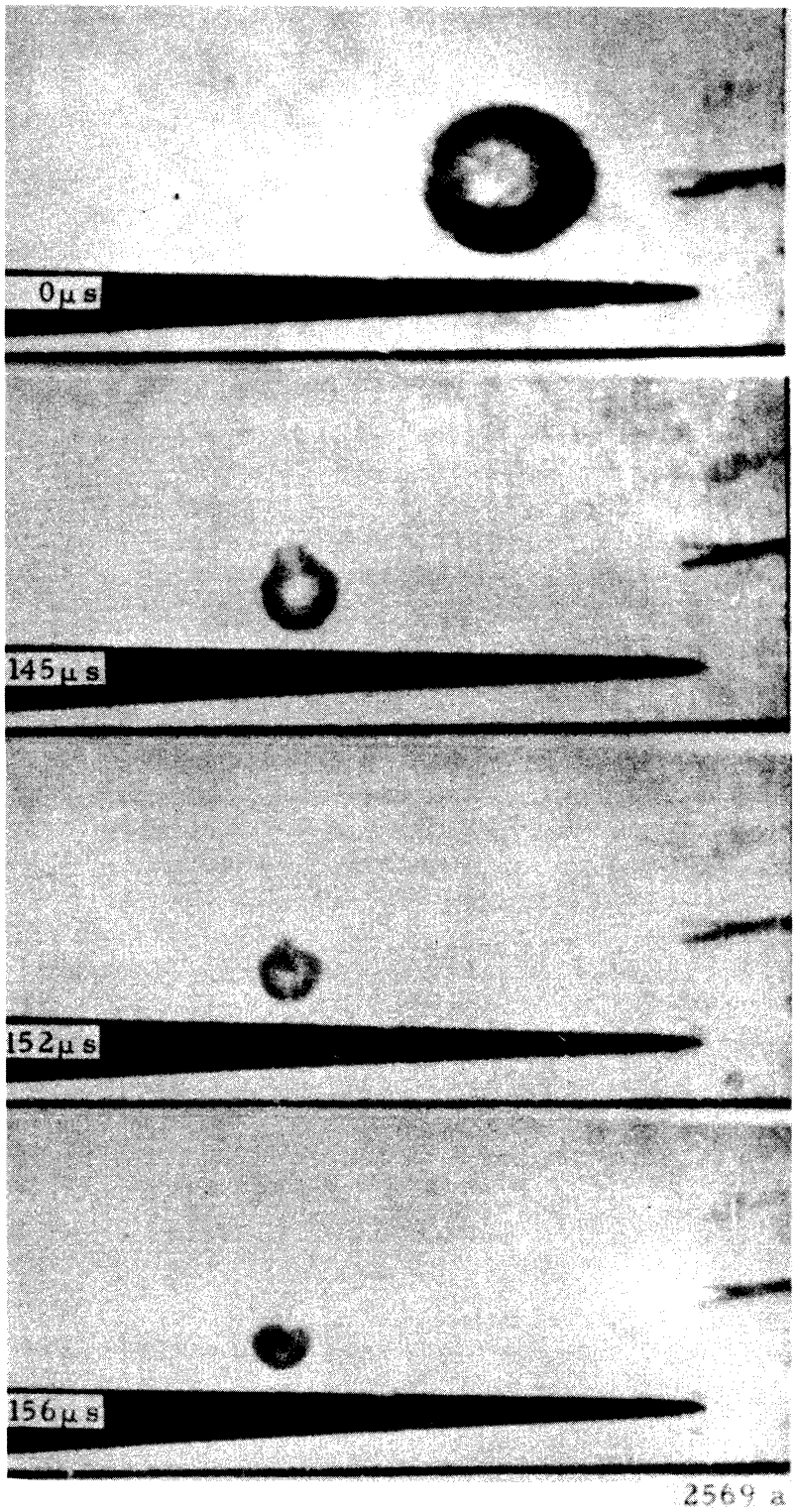

Figure 4a. Model 330 High Speed Photographs of a Spark Induced Cavitation Bubble Collapsing in the Modified Aluminum Two-Dimensional Venturi. Diffuse Back Lighting, Time Measured from the First Frame, 1.8 μs Exposure/Frame, Fluid Velocity 26.7 m/s, Right to Left, Initial Normalized Wall Distance, h = 1.62, Magnification 5.0, Air Content 0.8%.

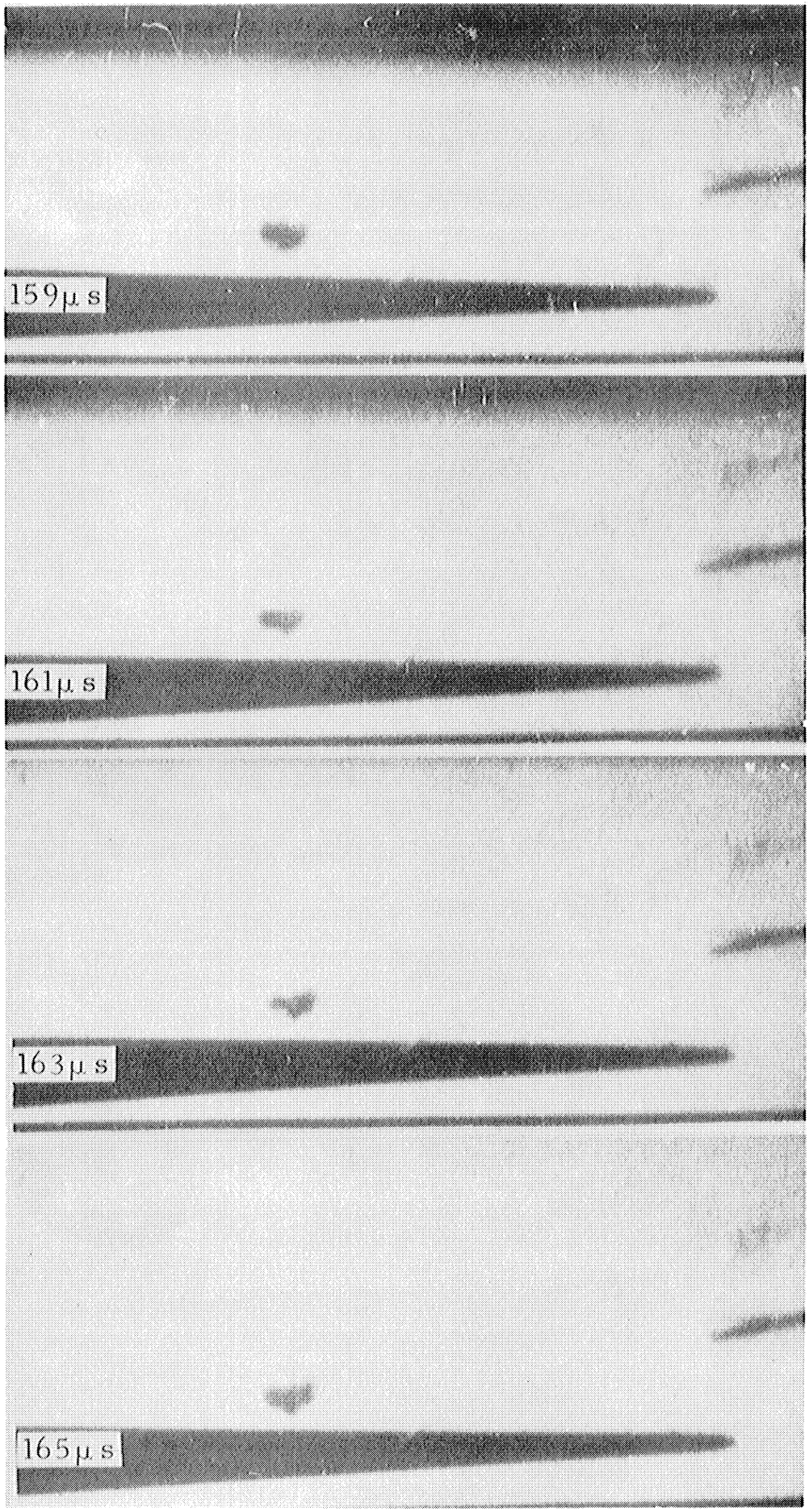

Figure 4b. Continued 2569 b

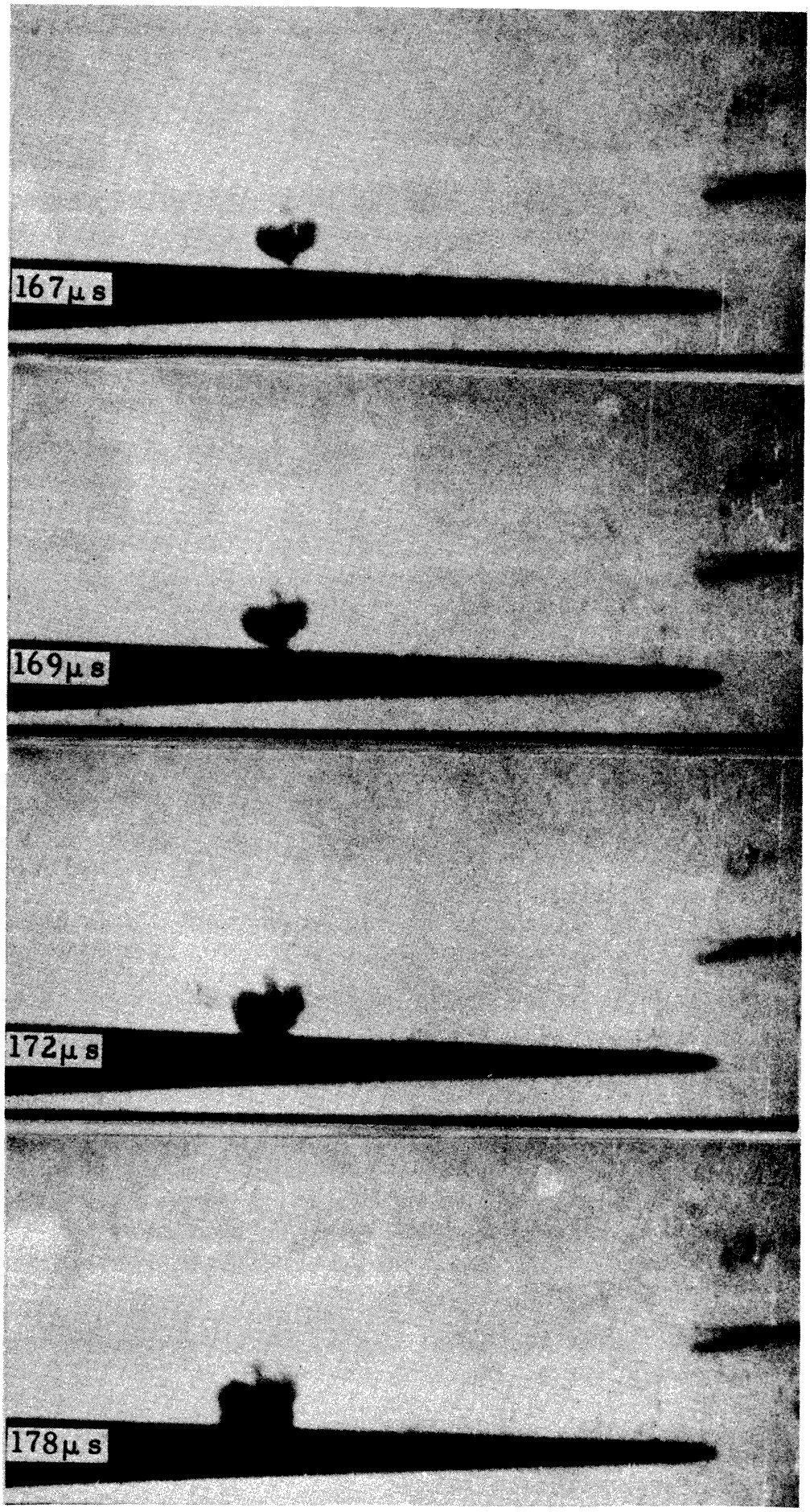

2569 c

Figure 4c. Continued

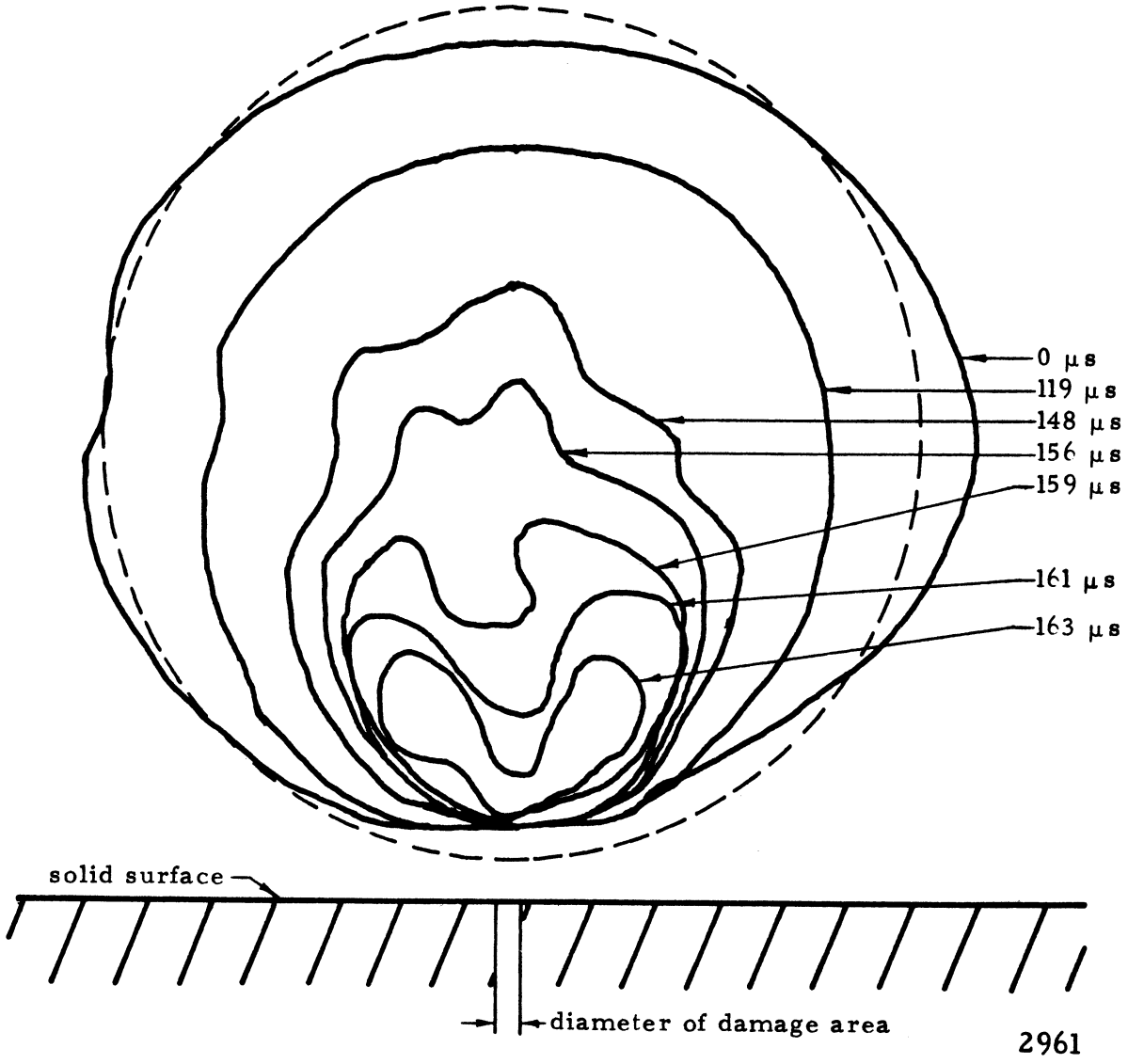

Figure 5a. Outlines of the Spark Induced Cavitation Bubble 4 at Various Stages of Collapse Showing the Mode of Deformation.

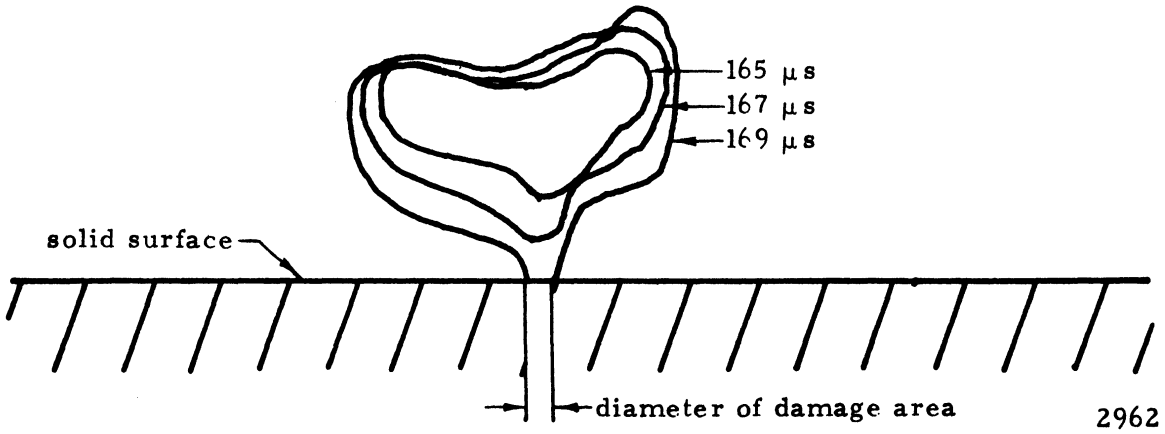

Figure 5b. Outlines of the Spark Induced Cavitation Bubble 4 at Various Stages of Rebound Showing the Bubble Impinging on the Nearby Solid Surface.

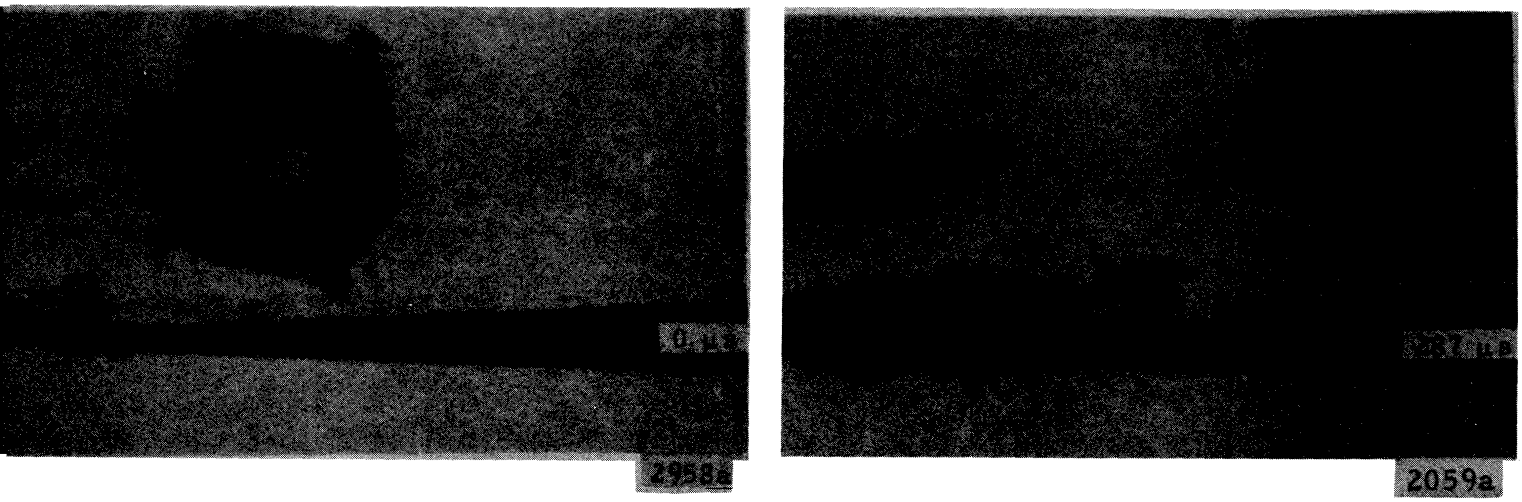

Figure 6a. Model 330 High Speed Photographs of Spark Induced Cavitation Bubble Breaking up in the Modified Aluminum Two-Dimensional Venturi. Diffuse Back Lighting, Time Measured from First Frame, 5.1 μs Exposure/Frame, Fluid Velocity 24.7 m/s Left to Right, Initial Normalized Wall Distance, h = 1.35, Magn. 7.5. Air Content 0.6%.

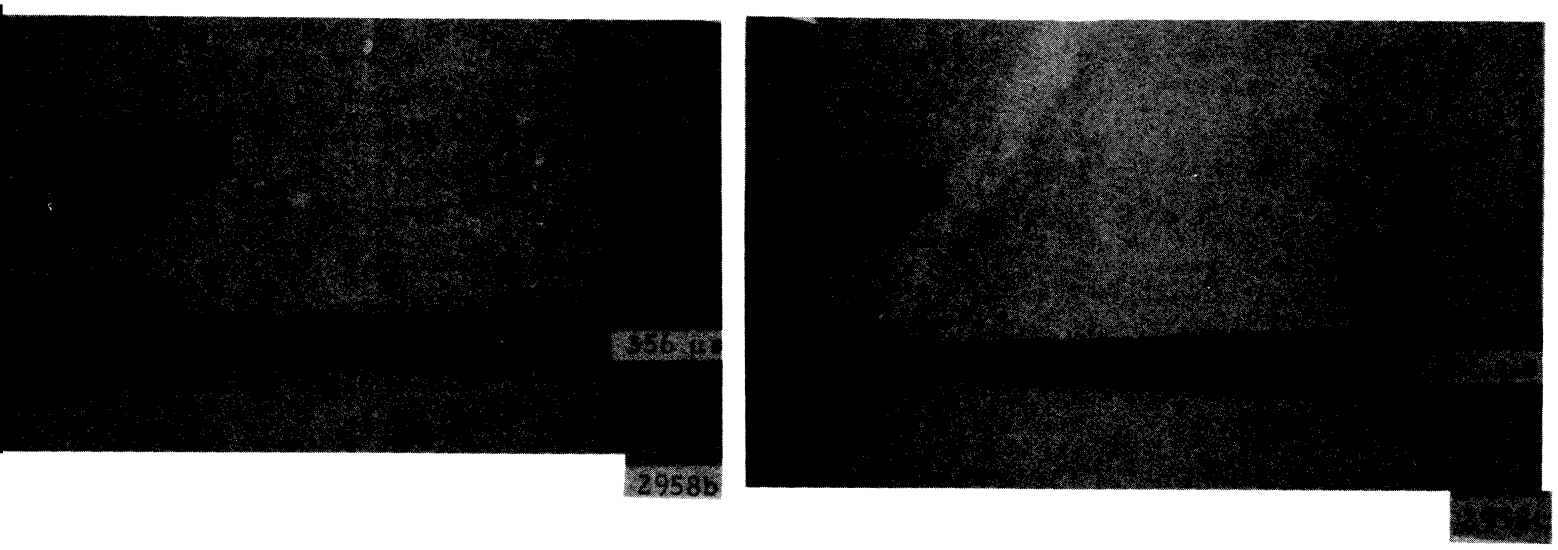

Figure 6b. Continued

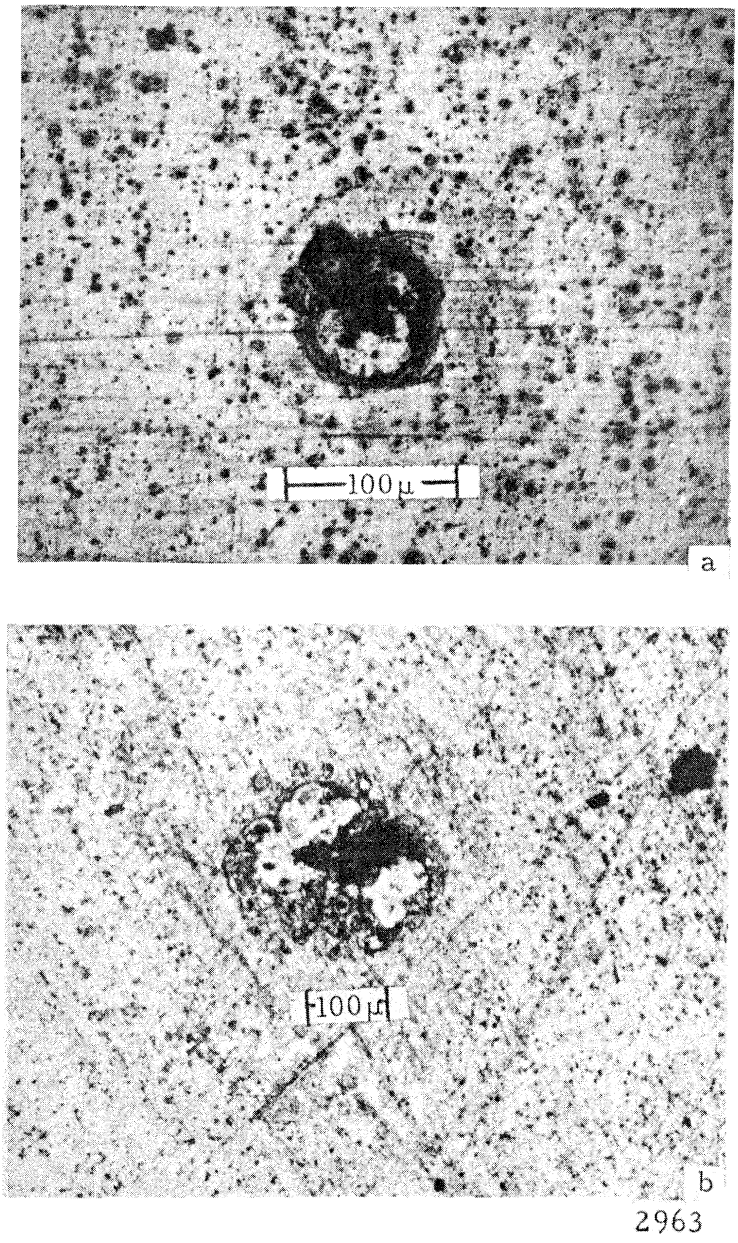

Figure 7a. Photomicrographs of the Damage Produced on the 50 μ Thick Aluminum Foil During the Collapse and Rebound of Bubble Figure 4, Scale as shown.

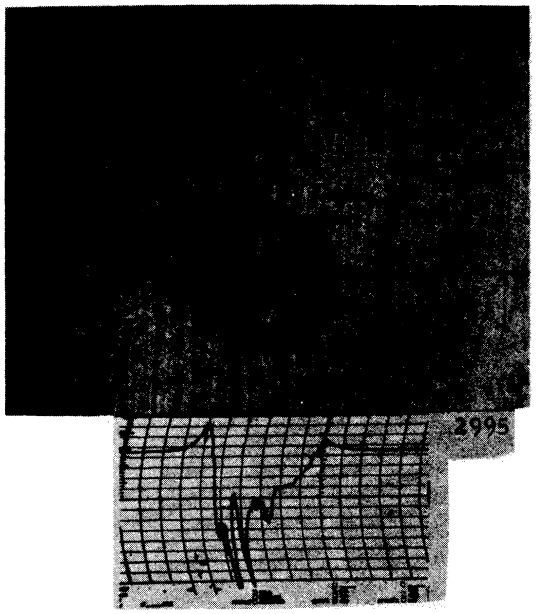

Figure 7b. Pit Produced in 1100-0 Aluminum
Impact of High Speed Liquid Jet
(670 m/sec., .18 cm. dia. jet)
Proficorder Graduations: 660 μ
Horizontal, 6.35 μ Vertical.

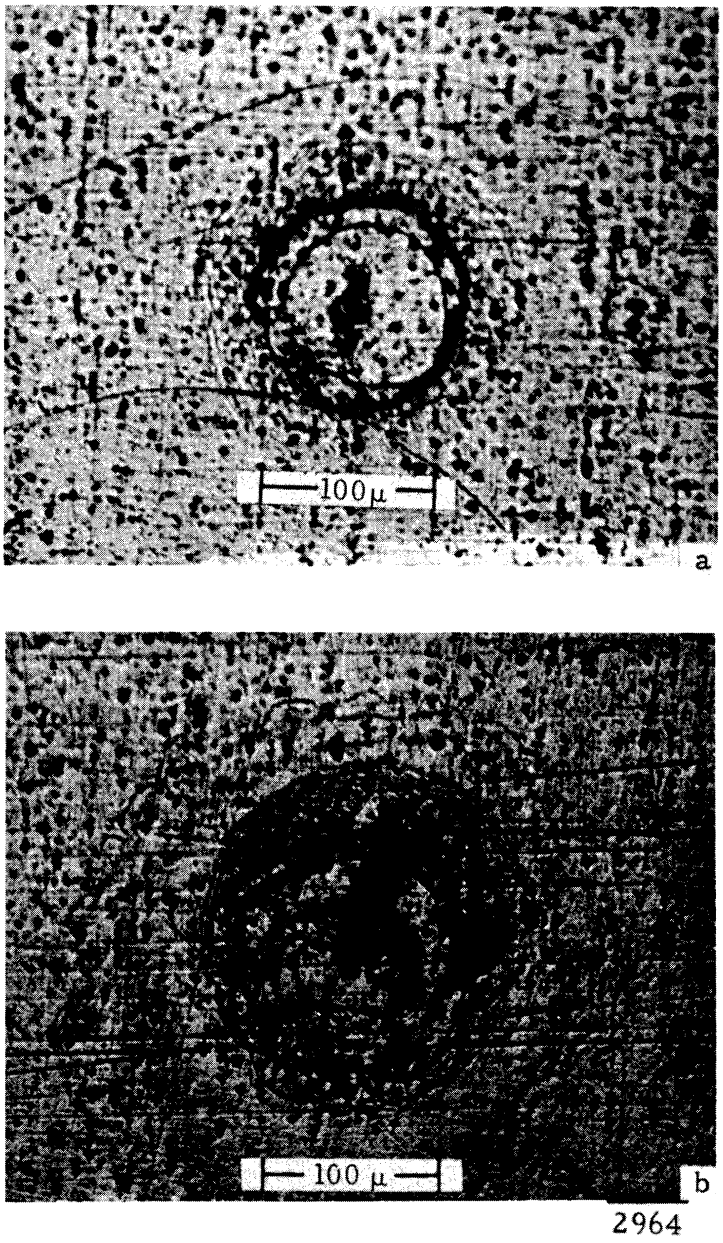

Figure 7c. Photomicrographs of the Damage Produced on the 50 μ thick Aluminum Foil by the Initiating Spark of Bubble Fig. 4.

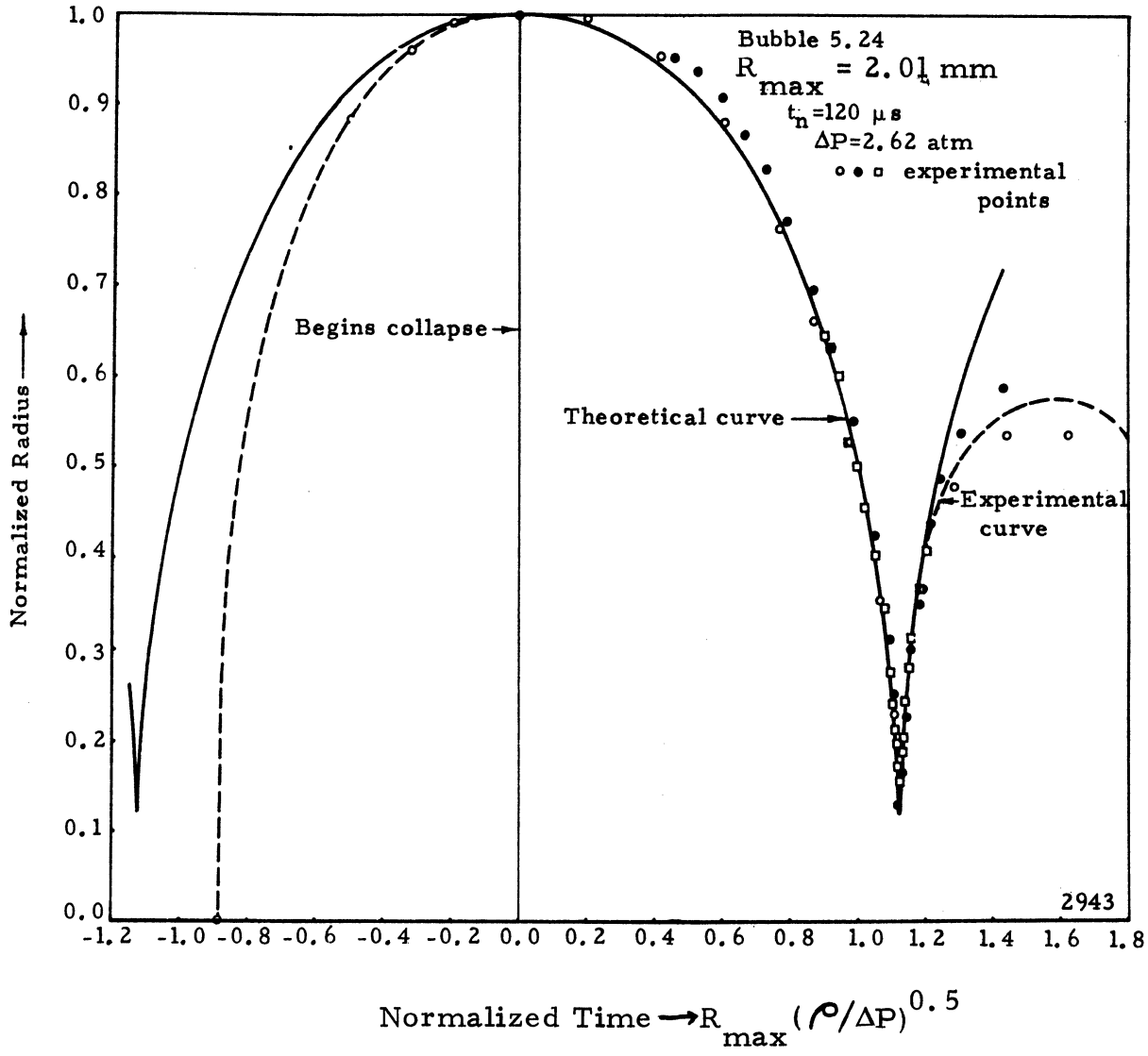

Figure 8a. Normalized Radius vs. Normalized Time for the Spark Induced Cavitation Bubble Shown in Figure 3.

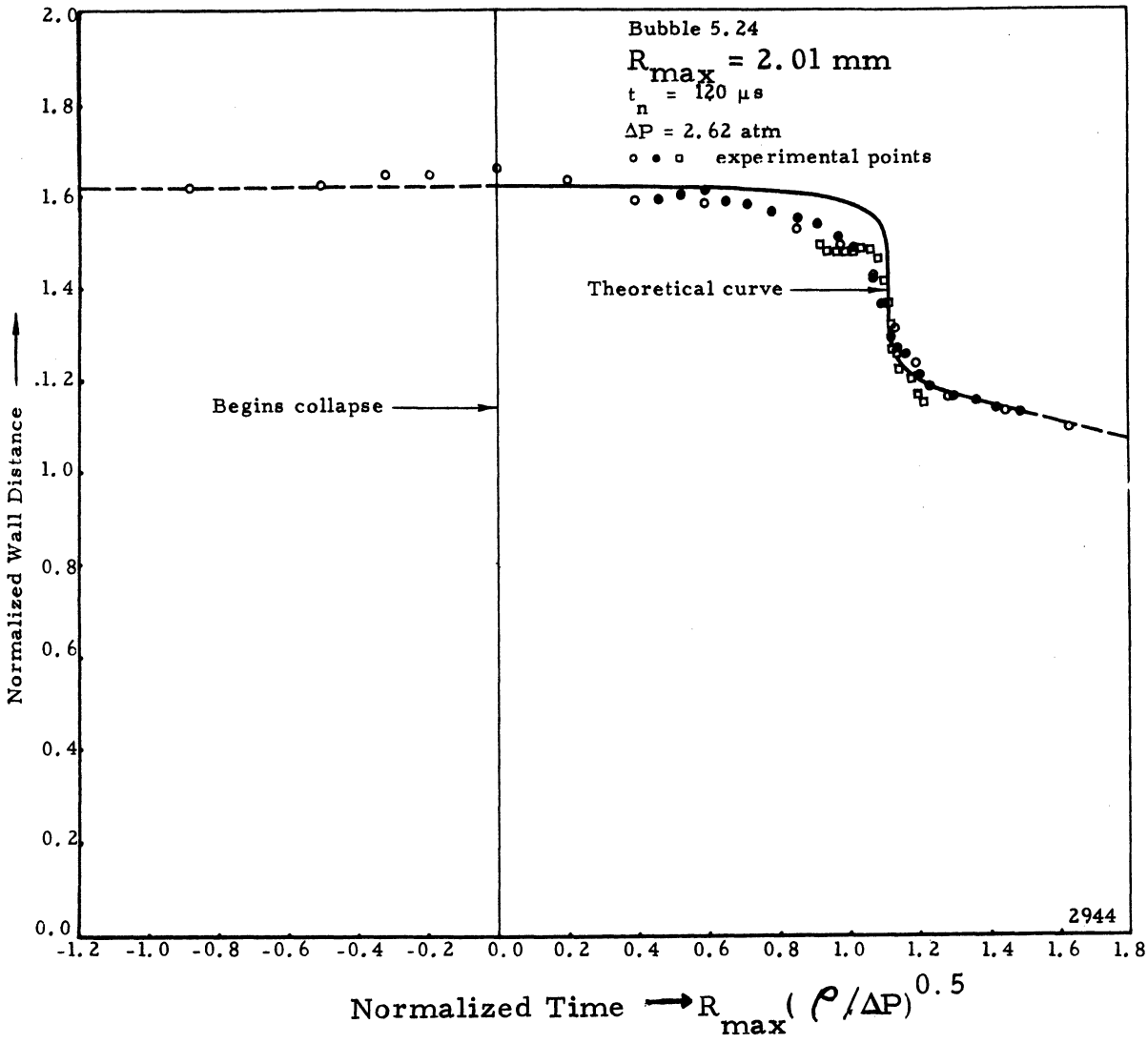

Figure 8b. Normalized Wall Distance vs. Normalized Time for the Spark Induced Cavitation Bubble Shown in Figure 3.

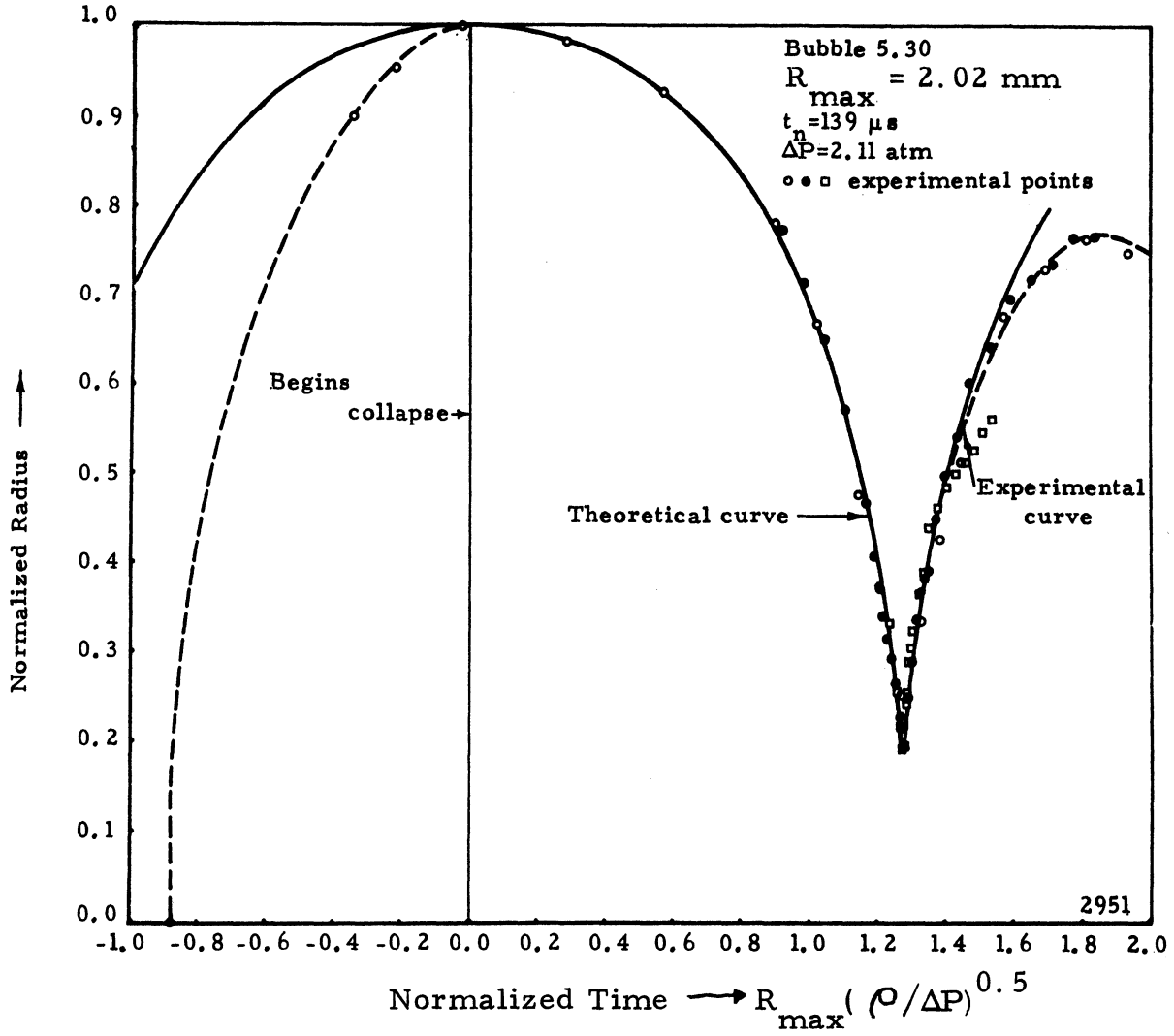

Figure 9a. Normalized Radius vs. Normalized Time for the Spark Induced Cavitation Bubble Shown in Figure 3.

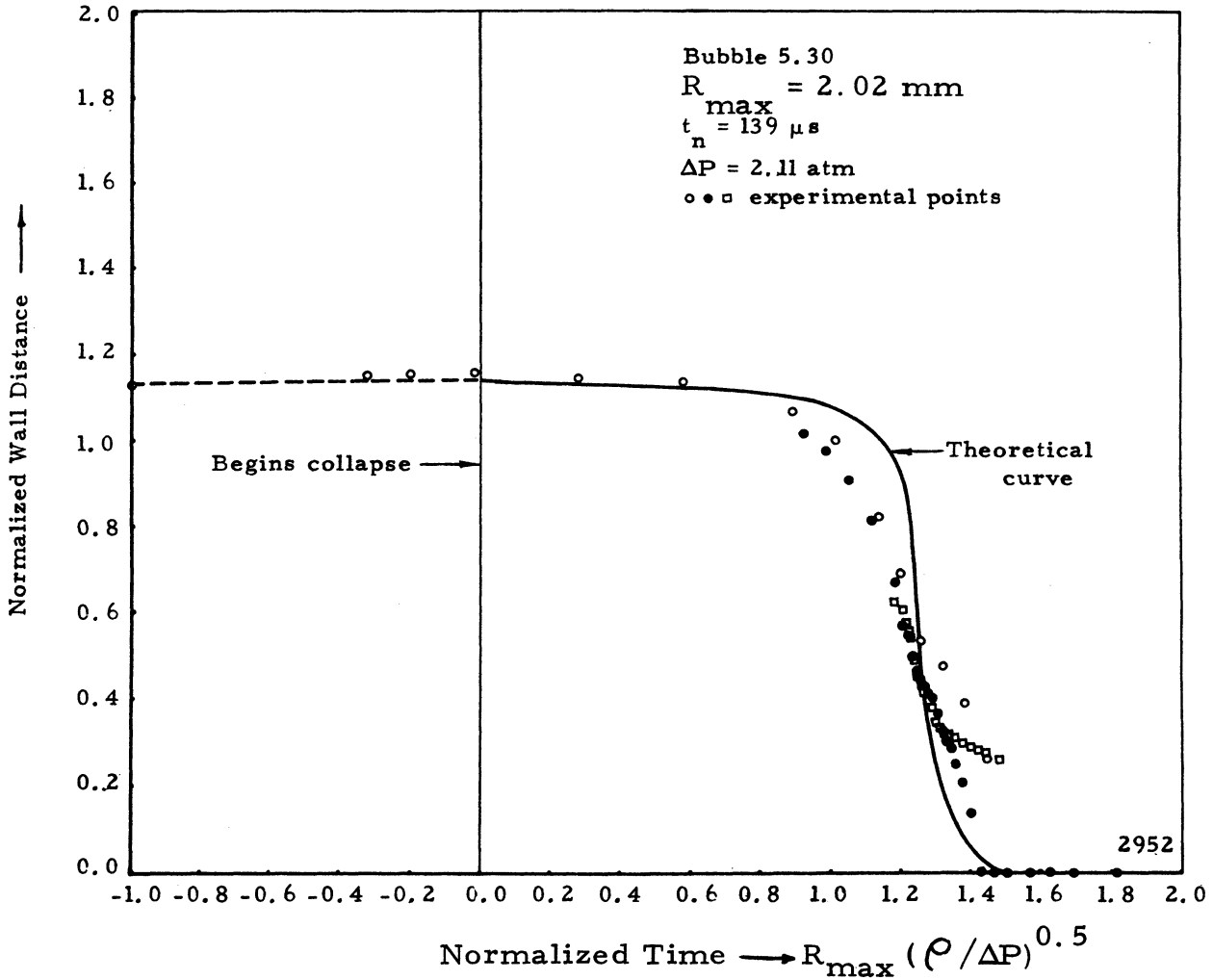

Figure 9b. Normalized Wall Distance vs. Normalized Time for the Spark Induced Cavitation Bubble Shown in Figure 4.

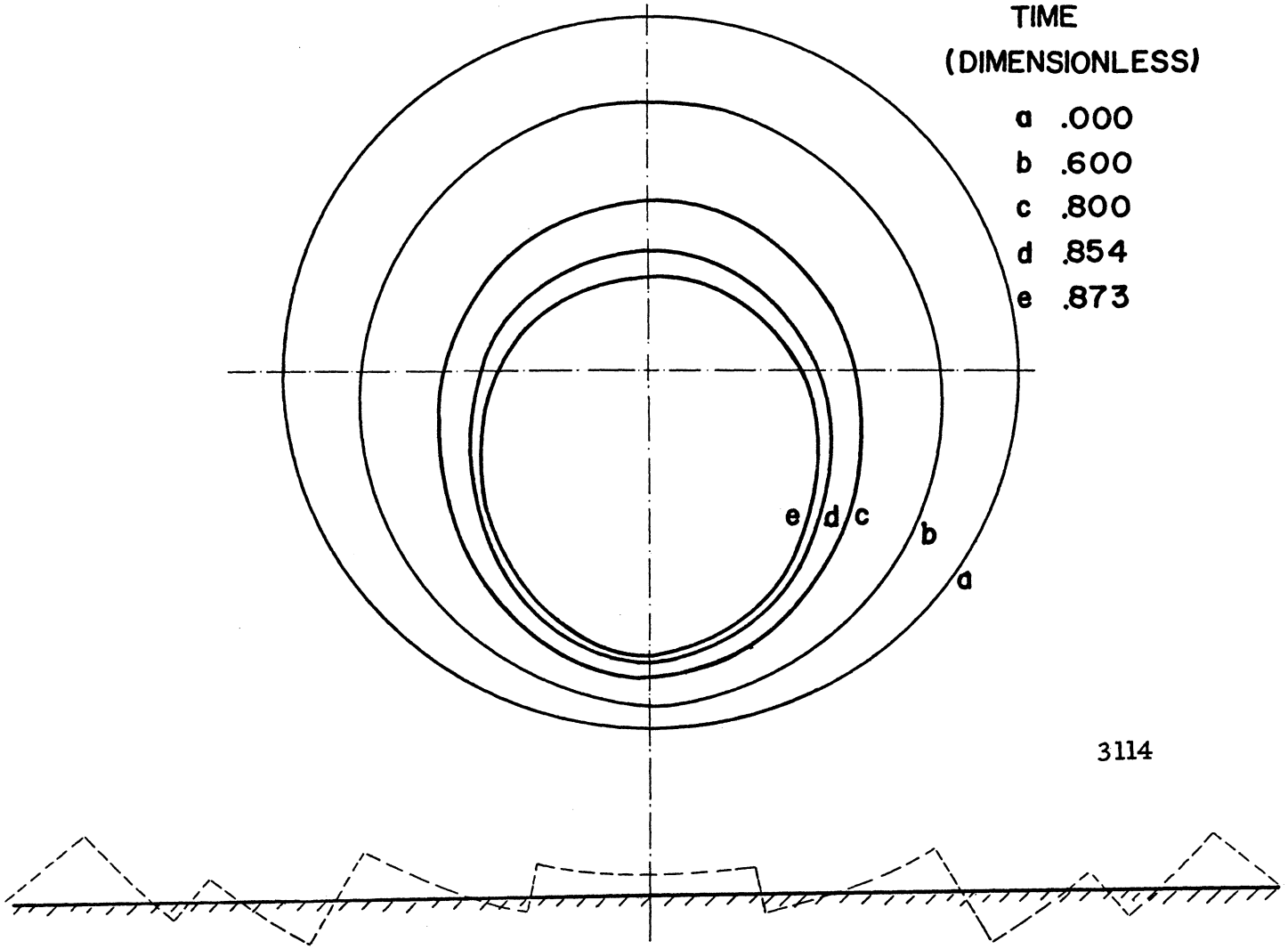

Figure 1 Bubble Surface Profiles for Initially Spherical Bubble with Center 1.5 R_o from Rigid Wall